

DESY 06-039  
April 2006

# Measurement of Charm and Beauty Dijet Cross Sections in Photoproduction at HERA using the H1 Vertex Detector

H1 Collaboration

## Abstract

A measurement of charm and beauty dijet photoproduction cross sections at the  $ep$  collider HERA is presented. Events are selected with two or more jets of transverse momentum  $p_t^{\text{jet}_{1(2)}} > 11(8)$  GeV in the central range of pseudo-rapidity  $-0.9 < \eta^{\text{jet}_{1(2)}} < 1.3$ . The fractions of events containing charm and beauty quarks are determined using a method based on the impact parameter, in the transverse plane, of tracks to the primary vertex, as measured by the H1 central vertex detector. Differential dijet cross sections for charm and beauty, and their relative contributions to the flavour inclusive dijet photoproduction cross section, are measured as a function of the transverse momentum of the leading jet, the average pseudo-rapidity of the two jets and the observable  $x_\gamma^{\text{obs}}$ . Taking into account the theoretical uncertainties, the charm cross sections are consistent with a QCD calculation in next-to-leading order, while the predicted cross sections for beauty production are somewhat lower than the measurement.

Submitted to Eur. Phys. J. C

A. Aktas<sup>9</sup>, V. Andreev<sup>25</sup>, T. Anthonis<sup>3</sup>, B. Antunovic<sup>26</sup>, S. Aplin<sup>9</sup>, A. Asmone<sup>33</sup>, A. Astvatsatourov<sup>3</sup>, A. Babaev<sup>24,†</sup>, S. Backovic<sup>30</sup>, A. Baghdasaryan<sup>37</sup>, P. Baranov<sup>25</sup>, E. Barrelet<sup>29</sup>, W. Bartel<sup>9</sup>, S. Baudrand<sup>27</sup>, S. Baumgartner<sup>39</sup>, J. Becker<sup>40</sup>, M. Beckingham<sup>9</sup>, O. Behnke<sup>12</sup>, O. Behrendt<sup>6</sup>, A. Belousov<sup>25</sup>, N. Berger<sup>39</sup>, J.C. Bizot<sup>27</sup>, M.-O. Boenig<sup>6</sup>, V. Boudry<sup>28</sup>, J. Bracinik<sup>26</sup>, G. Brandt<sup>12</sup>, V. Brisson<sup>27</sup>, D. Bruncko<sup>15</sup>, F.W. Büsler<sup>10</sup>, A. Bunyatyan<sup>11,37</sup>, G. Buschhorn<sup>26</sup>, L. Bystritskaya<sup>24</sup>, A.J. Campbell<sup>9</sup>, F. Cassol-Brunner<sup>21</sup>, K. Cerny<sup>32</sup>, V. Cerny<sup>15,46</sup>, V. Chekelian<sup>26</sup>, J.G. Contreras<sup>22</sup>, J.A. Coughlan<sup>4</sup>, B.E. Cox<sup>20</sup>, G. Cozzika<sup>8</sup>, J. Cvach<sup>31</sup>, J.B. Dainton<sup>17</sup>, W.D. Dau<sup>14</sup>, K. Daum<sup>36,42</sup>, Y. de Boer<sup>24</sup>, B. Delcourt<sup>27</sup>, M. Del Degan<sup>39</sup>, A. De Roeck<sup>9,44</sup>, E.A. De Wolf<sup>3</sup>, C. Diaconu<sup>21</sup>, V. Dodonov<sup>11</sup>, A. Dubak<sup>30,45</sup>, G. Eckerlin<sup>9</sup>, V. Efremenko<sup>24</sup>, S. Egli<sup>35</sup>, R. Eichler<sup>35</sup>, F. Eisele<sup>12</sup>, A. Eliseev<sup>25</sup>, E. Elsen<sup>9</sup>, S. Essenov<sup>24</sup>, A. Falkewicz<sup>5</sup>, P.J.W. Faulkner<sup>2</sup>, L. Favart<sup>3</sup>, A. Fedotov<sup>24</sup>, R. Felst<sup>9</sup>, J. Feltesse<sup>8</sup>, J. Ferencei<sup>15</sup>, L. Finke<sup>10</sup>, M. Fleischer<sup>9</sup>, G. Flucke<sup>33</sup>, A. Fomenko<sup>25</sup>, G. Franke<sup>9</sup>, T. Frisson<sup>28</sup>, E. Gabathuler<sup>17</sup>, E. Garutti<sup>9</sup>, J. Gayler<sup>9</sup>, C. Gerlich<sup>12</sup>, S. Ghazaryan<sup>37</sup>, S. Ginzburgskaya<sup>24</sup>, A. Glazov<sup>9</sup>, I. Glushkov<sup>38</sup>, L. Goerlich<sup>5</sup>, M. Goettlich<sup>9</sup>, N. Gogitidze<sup>25</sup>, S. Gorbounov<sup>38</sup>, C. Grab<sup>39</sup>, T. Greenshaw<sup>17</sup>, M. Gregori<sup>18</sup>, B.R. Grell<sup>9</sup>, G. Grindhammer<sup>26</sup>, C. Gwilliam<sup>20</sup>, D. Haidt<sup>9</sup>, L. Hajduk<sup>5</sup>, M. Hansson<sup>19</sup>, G. Heinzelmann<sup>10</sup>, R.C.W. Henderson<sup>16</sup>, H. Henschel<sup>38</sup>, G. Herrera<sup>23</sup>, M. Hildebrandt<sup>35</sup>, K.H. Hiller<sup>38</sup>, D. Hoffmann<sup>21</sup>, R. Horisberger<sup>35</sup>, A. Hovhannisyan<sup>37</sup>, T. Hreus<sup>3,43</sup>, S. Hussain<sup>18</sup>, M. Ibbotson<sup>20</sup>, M. Ismail<sup>20</sup>, M. Jacquet<sup>27</sup>, L. Janauschek<sup>26</sup>, X. Janssen<sup>3</sup>, V. Jemanov<sup>10</sup>, L. Jönsson<sup>19</sup>, D.P. Johnson<sup>3</sup>, A.W. Jung<sup>13</sup>, H. Jung<sup>19,9</sup>, M. Kapichine<sup>7</sup>, J. Katzy<sup>9</sup>, I.R. Kenyon<sup>2</sup>, C. Kiesling<sup>26</sup>, M. Klein<sup>38</sup>, C. Kleinwort<sup>9</sup>, T. Klimkovich<sup>9</sup>, T. Kluge<sup>9</sup>, G. Knies<sup>9</sup>, A. Knutsson<sup>19</sup>, V. Korbel<sup>9</sup>, P. Kostka<sup>38</sup>, K. Krastev<sup>9</sup>, J. Kretschmar<sup>38</sup>, A. Kropivnitskaya<sup>24</sup>, K. Krüger<sup>13</sup>, M.P.J. Landon<sup>18</sup>, W. Lange<sup>38</sup>, G. Laštovička-Medin<sup>30</sup>, P. Laycock<sup>17</sup>, A. Lebedev<sup>25</sup>, G. Leibenguth<sup>39</sup>, V. Lendermann<sup>13</sup>, S. Levonian<sup>9</sup>, L. Lindfeld<sup>40</sup>, K. Lipka<sup>38</sup>, A. Liptaj<sup>26</sup>, B. List<sup>39</sup>, J. List<sup>10</sup>, E. Lobodzinska<sup>38,5</sup>, N. Loktionova<sup>25</sup>, R. Lopez-Fernandez<sup>23</sup>, V. Lubimov<sup>24</sup>, A.-I. Lucaci-Timoce<sup>9</sup>, H. Lueders<sup>10</sup>, D. Lüke<sup>6,9</sup>, T. Lux<sup>10</sup>, L. Lytkin<sup>11</sup>, A. Makankine<sup>7</sup>, N. Malden<sup>20</sup>, E. Malinovski<sup>25</sup>, S. Mangano<sup>39</sup>, P. Marage<sup>3</sup>, R. Marshall<sup>20</sup>, L. Marti<sup>9</sup>, M. Martisikova<sup>9</sup>, H.-U. Martyn<sup>1</sup>, S.J. Maxfield<sup>17</sup>, A. Mehta<sup>17</sup>, K. Meier<sup>13</sup>, A.B. Meyer<sup>9</sup>, H. Meyer<sup>36</sup>, J. Meyer<sup>9</sup>, V. Michels<sup>9</sup>, S. Mikocki<sup>5</sup>, I. Milcewicz-Mika<sup>5</sup>, D. Milstead<sup>17</sup>, D. Mladenov<sup>34</sup>, A. Mohamed<sup>17</sup>, F. Moreau<sup>28</sup>, A. Morozov<sup>7</sup>, J.V. Morris<sup>4</sup>, M.U. Mozer<sup>12</sup>, K. Müller<sup>40</sup>, P. Murín<sup>15,43</sup>, K. Nankov<sup>34</sup>, B. Naroska<sup>10</sup>, Th. Naumann<sup>38</sup>, P.R. Newman<sup>2</sup>, C. Niebuhr<sup>9</sup>, A. Nikiforov<sup>26</sup>, G. Nowak<sup>5</sup>, K. Nowak<sup>40</sup>, M. Nozicka<sup>32</sup>, R. Oganezov<sup>37</sup>, B. Olivier<sup>26</sup>, J.E. Olsson<sup>9</sup>, S. Osman<sup>19</sup>, D. Ozerov<sup>24</sup>, V. Palichik<sup>7</sup>, I. Panagoulas<sup>9</sup>, T. Papadopoulou<sup>9</sup>, C. Pascaud<sup>27</sup>, G.D. Patel<sup>17</sup>, H. Peng<sup>9</sup>, E. Perez<sup>8</sup>, D. Perez-Astudillo<sup>22</sup>, A. Perieanu<sup>9</sup>, A. Petrukhin<sup>24</sup>, D. Pitzl<sup>9</sup>, R. Plačákytė<sup>26</sup>, B. Portheault<sup>27</sup>, B. Povh<sup>11</sup>, P. Prideaux<sup>17</sup>, A.J. Rahmat<sup>17</sup>, N. Raicevic<sup>30</sup>, P. Reimer<sup>31</sup>, A. Rimmer<sup>17</sup>, C. Rislér<sup>9</sup>, E. Rizvi<sup>18</sup>, P. Robmann<sup>40</sup>, B. Roland<sup>3</sup>, R. Roosen<sup>3</sup>, A. Rostovtsev<sup>24</sup>, Z. Rurikova<sup>26</sup>, S. Rusakov<sup>25</sup>, F. Salvaire<sup>10</sup>, D.P.C. Sankey<sup>4</sup>, E. Sauvan<sup>21</sup>, S. Schätzel<sup>9</sup>, S. Schmidt<sup>9</sup>, S. Schmitt<sup>9</sup>, C. Schmitz<sup>40</sup>, L. Schoeffel<sup>8</sup>, A. Schöning<sup>39</sup>, H.-C. Schultz-Coulon<sup>13</sup>, F. Sefkow<sup>9</sup>, R.N. Shaw-West<sup>2</sup>, I. Sheviakov<sup>25</sup>, L.N. Shtarkov<sup>25</sup>, T. Sloan<sup>16</sup>, P. Smirnov<sup>25</sup>, Y. Soloviev<sup>25</sup>, D. South<sup>9</sup>, V. Spaskov<sup>7</sup>, A. Specka<sup>28</sup>, M. Steder<sup>9</sup>, B. Stella<sup>33</sup>, J. Stiewe<sup>13</sup>, A. Stoilov<sup>34</sup>, U. Straumann<sup>40</sup>, D. Sunar<sup>3</sup>, V. Tchoulakov<sup>7</sup>, G. Thompson<sup>18</sup>, P.D. Thompson<sup>2</sup>, T. Toll<sup>9</sup>, F. Tomasz<sup>15</sup>, D. Traynor<sup>18</sup>, P. Truöl<sup>40</sup>, I. Tsakov<sup>34</sup>, G. Tsipolitis<sup>9,41</sup>, I. Tsurin<sup>9</sup>, J. Turnau<sup>5</sup>, E. Tzamariudaki<sup>26</sup>, K. Urban<sup>13</sup>, M. Urban<sup>40</sup>, A. Usik<sup>25</sup>, D. Utkin<sup>24</sup>, A. Valkárová<sup>32</sup>, C. Vallée<sup>21</sup>, P. Van Mechelen<sup>3</sup>, A. Vargas Trevino<sup>6</sup>, Y. Vazdik<sup>25</sup>, C. Veelken<sup>17</sup>, S. Vinokurova<sup>9</sup>, V. Volchinski<sup>37</sup>, K. Wacker<sup>6</sup>, G. Weber<sup>10</sup>, R. Weber<sup>39</sup>, D. Wegener<sup>6</sup>, C. Werner<sup>12</sup>, M. Wessels<sup>9</sup>, B. Wessling<sup>9</sup>, Ch. Wissing<sup>6</sup>, R. Wolf<sup>12</sup>, E. Wunsch<sup>9</sup>, S. Xella<sup>40</sup>, W. Yan<sup>9</sup>, V. Yeganov<sup>37</sup>, J. Žáček<sup>32</sup>, J. Zálešák<sup>31</sup>, Z. Zhang<sup>27</sup>, A. Zhelezov<sup>24</sup>, A. Zhokin<sup>24</sup>, Y.C. Zhu<sup>9</sup>, J. Zimmermann<sup>26</sup>, T. Zimmermann<sup>39</sup>, H. Zohrabyan<sup>37</sup>, and F. Zomer<sup>27</sup>

- <sup>1</sup> *I. Physikalisches Institut der RWTH, Aachen, Germany<sup>a</sup>*
- <sup>2</sup> *School of Physics and Astronomy, University of Birmingham, Birmingham, UK<sup>b</sup>*
- <sup>3</sup> *Inter-University Institute for High Energies ULB-VUB, Brussels; Universiteit Antwerpen, Antwerpen; Belgium<sup>c</sup>*
- <sup>4</sup> *Rutherford Appleton Laboratory, Chilton, Didcot, UK<sup>b</sup>*
- <sup>5</sup> *Institute for Nuclear Physics, Cracow, Poland<sup>d</sup>*
- <sup>6</sup> *Institut für Physik, Universität Dortmund, Dortmund, Germany<sup>a</sup>*
- <sup>7</sup> *Joint Institute for Nuclear Research, Dubna, Russia*
- <sup>8</sup> *CEA, DSM/DAPNIA, CE-Saclay, Gif-sur-Yvette, France*
- <sup>9</sup> *DESY, Hamburg, Germany*
- <sup>10</sup> *Institut für Experimentalphysik, Universität Hamburg, Hamburg, Germany<sup>a</sup>*
- <sup>11</sup> *Max-Planck-Institut für Kernphysik, Heidelberg, Germany*
- <sup>12</sup> *Physikalisches Institut, Universität Heidelberg, Heidelberg, Germany<sup>a</sup>*
- <sup>13</sup> *Kirchhoff-Institut für Physik, Universität Heidelberg, Heidelberg, Germany<sup>a</sup>*
- <sup>14</sup> *Institut für Experimentelle und Angewandte Physik, Universität Kiel, Kiel, Germany*
- <sup>15</sup> *Institute of Experimental Physics, Slovak Academy of Sciences, Košice, Slovak Republic<sup>f</sup>*
- <sup>16</sup> *Department of Physics, University of Lancaster, Lancaster, UK<sup>b</sup>*
- <sup>17</sup> *Department of Physics, University of Liverpool, Liverpool, UK<sup>b</sup>*
- <sup>18</sup> *Queen Mary and Westfield College, London, UK<sup>b</sup>*
- <sup>19</sup> *Physics Department, University of Lund, Lund, Sweden<sup>g</sup>*
- <sup>20</sup> *Physics Department, University of Manchester, Manchester, UK<sup>b</sup>*
- <sup>21</sup> *CPPM, CNRS/IN2P3 - Univ. Mediterranee, Marseille - France*
- <sup>22</sup> *Departamento de Física Aplicada, CINVESTAV, Mérida, Yucatán, México<sup>j</sup>*
- <sup>23</sup> *Departamento de Física, CINVESTAV, México<sup>j</sup>*
- <sup>24</sup> *Institute for Theoretical and Experimental Physics, Moscow, Russia<sup>k</sup>*
- <sup>25</sup> *Lebedev Physical Institute, Moscow, Russia<sup>e</sup>*
- <sup>26</sup> *Max-Planck-Institut für Physik, München, Germany*
- <sup>27</sup> *LAL, Université de Paris-Sud 11, IN2P3-CNRS, Orsay, France*
- <sup>28</sup> *LLR, Ecole Polytechnique, IN2P3-CNRS, Palaiseau, France*
- <sup>29</sup> *LPNHE, Universités Paris VI and VII, IN2P3-CNRS, Paris, France*
- <sup>30</sup> *Faculty of Science, University of Montenegro, Podgorica, Serbia and Montenegro<sup>e</sup>*
- <sup>31</sup> *Institute of Physics, Academy of Sciences of the Czech Republic, Praha, Czech Republic<sup>h</sup>*
- <sup>32</sup> *Faculty of Mathematics and Physics, Charles University, Praha, Czech Republic<sup>h</sup>*
- <sup>33</sup> *Dipartimento di Fisica Università di Roma Tre and INFN Roma 3, Roma, Italy*
- <sup>34</sup> *Institute for Nuclear Research and Nuclear Energy, Sofia, Bulgaria<sup>e</sup>*
- <sup>35</sup> *Paul Scherrer Institut, Villigen, Switzerland*
- <sup>36</sup> *Fachbereich C, Universität Wuppertal, Wuppertal, Germany*
- <sup>37</sup> *Yerevan Physics Institute, Yerevan, Armenia*
- <sup>38</sup> *DESY, Zeuthen, Germany*
- <sup>39</sup> *Institut für Teilchenphysik, ETH, Zürich, Switzerland<sup>i</sup>*
- <sup>40</sup> *Physik-Institut der Universität Zürich, Zürich, Switzerland<sup>i</sup>*
  
- <sup>41</sup> *Also at Physics Department, National Technical University, Zografou Campus, GR-15773 Athens, Greece*
- <sup>42</sup> *Also at Rechenzentrum, Universität Wuppertal, Wuppertal, Germany*

<sup>43</sup> Also at University of P.J. Šafárik, Košice, Slovak Republic

<sup>44</sup> Also at CERN, Geneva, Switzerland

<sup>45</sup> Also at Max-Planck-Institut für Physik, München, Germany

<sup>46</sup> Also at Comenius University, Bratislava, Slovak Republic

† Deceased

<sup>a</sup> Supported by the Bundesministerium für Bildung und Forschung, FRG, under contract numbers 05 H1 1GUA /1, 05 H1 1PAA /1, 05 H1 1PAB /9, 05 H1 1PEA /6, 05 H1 1VHA /7 and 05 H1 1VHB /5

<sup>b</sup> Supported by the UK Particle Physics and Astronomy Research Council, and formerly by the UK Science and Engineering Research Council

<sup>c</sup> Supported by FNRS-FWO-Vlaanderen, IISN-IKW and IWT and by Interuniversity Attraction Poles Programme, Belgian Science Policy

<sup>d</sup> Partially Supported by the Polish State Committee for Scientific Research, SPUB/DESY/P003/DZ 118/2003/2005

<sup>e</sup> Supported by the Deutsche Forschungsgemeinschaft

<sup>f</sup> Supported by VEGA SR grant no. 2/4067/24

<sup>g</sup> Supported by the Swedish Natural Science Research Council

<sup>h</sup> Supported by the Ministry of Education of the Czech Republic under the projects LC527 and INGO-1P05LA259

<sup>i</sup> Supported by the Swiss National Science Foundation

<sup>j</sup> Supported by CONACYT, México, grant 400073-F

<sup>k</sup> Partially Supported by Russian Foundation for Basic Research, grants 03-02-17291 and 04-02-16445

# 1 Introduction

A measurement is presented of charm and beauty production in  $ep$  collisions at HERA using events with two or more jets at high transverse momentum. The measurement is carried out in the photoproduction region in which a quasi-real photon, with virtuality  $Q^2 \sim 0$ , is emitted from the incoming positron and interacts with a parton from the proton. Differential charm and beauty dijet cross sections are measured and compared to calculations in perturbative quantum chromodynamics (pQCD) performed to next-to-leading order (NLO).

In pQCD calculations, the photoproduction of charm and beauty proceeds dominantly via the direct photon-gluon fusion process  $\gamma g \rightarrow c\bar{c}$  or  $b\bar{b}$ , where the photon interacts with a gluon from the proton to produce a pair of heavy quarks in the final state. Previous charm measurements have confirmed this prediction [1–4]. In leading order QCD models a successful description of the data is obtained when additional contributions from processes involving resolved photons are taken into account [2, 3]. In such resolved photon processes the quasi-real photon fluctuates into a hadronic state before the hard interaction and thus acts as a source of partons. In the massless scheme, a large fraction of these resolved photon processes is due to heavy quark excitation, in which one of the partons that enters the hard interaction is a heavy quark ( $c$  or  $b$ ) originating from the resolved photon or the proton.

In this analysis events containing heavy quarks are distinguished from light quark events by the long lifetimes of  $c$  and  $b$  flavoured hadrons, which lead to displacements of tracks from the primary vertex. This technique, based on the precise spatial information from the H1 silicon vertex detector, was introduced in recent H1 measurements of the charm and beauty structure functions  $F_2^{cc}$  and  $F_2^{bb}$  in deep inelastic scattering [5,6], and is now applied to dijet events in photoproduction. This analysis provides the first simultaneous measurement of charm and beauty in photoproduction, extending to larger values of transverse jet momentum than previous measurements [1–4, 7–10]. The regions of small transverse momentum and large pseudo-rapidities are excluded from the measurement, due to trigger requirements and the limited angular acceptance of the vertex detector.

The differential charm and beauty dijet cross sections are measured as functions of the transverse momentum of the leading jet  $p_t^{\text{jet}_1}$ , of the mean pseudo-rapidity  $\bar{\eta}$  of the two jets, and of the variable  $x_\gamma^{\text{obs}}$  which, in a leading order picture, corresponds to the fraction of the photon's energy in the proton rest frame that enters the hard interaction. For direct photon-gluon fusion processes  $x_\gamma^{\text{obs}} \sim 1$ , while for resolved photon processes  $x_\gamma^{\text{obs}}$  can be small. The measured differential charm and beauty cross sections, together with the measured flavour inclusive cross sections, are used to determine the relative contribution from charm and beauty events to dijet photoproduction. The results are compared with calculations in perturbative quantum chromodynamics at next-to-leading order and with predictions from Monte Carlo simulations in which leading order matrix elements are implemented, and contributions from higher orders are approximated using parton showers.

This paper is structured as follows: In section 2 the experimental apparatus is briefly described. Event and track selections are detailed in section 3. The method to determine the contributions of charm and beauty events is outlined in section 4. Theoretical calculations performed in the framework of perturbative QCD are discussed in section 5. The cross section

measurements and their systematic uncertainties are presented in section 6. Properties of a heavy quark enriched data sample are investigated in section 7. A summary of the results is given in section 8.

## 2 H1 Detector

The H1 detector is described in detail in [11]. Charged particles emerging from the  $ep$  interaction region are measured by the central tracking detector (CTD) in the pseudo-rapidity range  $-1.74 < \eta < 1.74$ <sup>1</sup>. The CTD consists of two large cylindrical central jet drift chambers (CJCs), two  $z$  chambers and two multi-wire proportional chambers arranged concentrically around the beam-line in a magnetic field of 1.15 T. The CTD provides triggering information based on track segments from the CJC in the  $r$ - $\phi$  plane, transverse to the beam direction, and on the  $z$  position of the vertex from the multi-wire proportional chambers. The CJC tracks are linked with hits in the Central Silicon Tracking detector (CST) [12], which consists of two cylindrical layers of silicon strip sensors, surrounding the beam pipe at radii of 57.5 mm and 97 mm from the beam axis. The detector provides hit resolutions of 12  $\mu\text{m}$  in  $r$ - $\phi$  with an average efficiency of 97%.

For CTD tracks with CST hits in both layers the impact parameter  $\delta$ , i.e. the transverse distance of closest approach to the nominal vertex, can be measured with a resolution of  $\sigma_\delta \approx 33 \mu\text{m} \oplus 90 \mu\text{m}/p_t[\text{GeV}]$ . The first term represents the intrinsic resolution and includes the uncertainty of the CST alignment, the second term corresponds to the contribution from multiple scattering in the beam pipe and the CST, which depends on the transverse momentum  $p_t$  of the track.

Charged and neutral particles are measured in the liquid argon (LAr) calorimeter which surrounds the tracking chambers and covers the range  $-1.5 < \eta < 3.4$  and a lead-scintillating fibre calorimeter SpaCal, covering the backward region ( $-4.0 < \eta < -1.4$ ) [13]. The measurements from CTD and calorimeters are combined to reconstruct the final state particles [14]. The luminosity determination is based on the measurement of the Bethe-Heitler process ( $ep \rightarrow ep\gamma$ ), where the photon is detected in a calorimeter located downstream of the interaction point in the positron beam direction.

## 3 Event and Track Selection

The data sample corresponds to an integrated luminosity of  $56.8 \text{ pb}^{-1}$  and was recorded with the H1 experiment during the years 1999 and 2000. During this time HERA was operated with positrons of 27.5 GeV energy and protons of 920 GeV. The events were triggered by a combination of signals from the calorimeters, the central drift chambers and the multi-wire proportional chambers. Photoproduction events are selected by requiring that there be no isolated high energy electromagnetic cluster detected in the calorimeters consistent with a signal from

---

<sup>1</sup>The pseudo-rapidity is given by  $\eta = -\ln \tan(\theta/2)$ , where  $\theta$  is measured with respect to the  $z$ -axis given by the proton beam direction.

the scattered positron. This restricts the range of negative four-momentum transfer squared to  $Q^2 < 1 \text{ GeV}^2$ . The inelasticity  $y$  is calculated using the hadronic final state [15], and the measurement is restricted to the range  $0.15 < y < 0.8$ . The jets are reconstructed from the final state particles using the inclusive  $k_t$  algorithm [16] in the  $p_t$  recombination scheme [17], with distance parameter  $R = 1$  in the  $\eta$ - $\phi$  plane. The event selection requires at least two jets in the central pseudo-rapidity range  $-0.9 < \eta < 1.3$  with transverse energy  $p_t^{\text{jet}_{1(2)}} > 11(8) \text{ GeV}$ .

CTD tracks are selected which are linked to hits in both  $r$ - $\phi$  layers of the CST. These tracks are required to have a transverse momentum above 500 MeV and a polar angle in the range  $30^\circ < \theta_{\text{track}} < 150^\circ$ . Events are selected which contain at least one selected track associated to one of the two leading jets. The final sample consists of 80769 events.

To correct for detector effects, such as detector resolutions and inefficiencies, large samples of charm, beauty and light quark events are generated using the Monte Carlo program PYTHIA [18] (for details see section 5). All samples are passed through a detailed simulation of the H1 detector response based on the GEANT program [19] and the same reconstruction and analysis algorithms as used for the data.

Figure 1 shows the distributions of the transverse momentum of the leading jet  $p_t^{\text{jet}_1}$ , and of the jet with the second highest transverse momentum  $p_t^{\text{jet}_2}$  (figures 1a and b), of the mean pseudo-rapidity  $\bar{\eta} = (\eta^{\text{jet}_1} + \eta^{\text{jet}_2})/2$  of the two jets (figure 1c) and of  $x_\gamma^{\text{obs}}$  (figure 1d). The observable  $x_\gamma^{\text{obs}}$  is defined as  $((E - p_z)_{\text{jet}_1} + (E - p_z)_{\text{jet}_2}) / \sum (E - p_z)$  where the sum runs over all measured particles of the final state. In figures 1e and f the transverse momentum and polar angular distributions of the selected tracks are shown. The simulation based on the PYTHIA event generator provides a good description of all distributions, after scaling the contributions from light quark, charm and beauty events. The scale factors are obtained from fits to the signed impact parameter distributions, as described below in section 4.

## 4 Quark Flavour Separation

The fractions of events containing charm and beauty quarks are determined using the same method as in previous measurements [5, 6], based on the impact parameter of selected tracks which is given by the transverse distance of closest approach to the reconstructed event vertex. The signed impact parameter  $\delta$  is defined as positive if the angle between the axis of the associated jet and the line joining the primary vertex to the point of closest approach of the track is less than  $90^\circ$ , and is defined as negative otherwise.

The distribution of  $\delta$  is shown in figure 2a. The data are well described by the simulation. Due to the long lifetimes of charm and beauty flavoured hadrons the  $\delta$  distribution is asymmetric, the number of tracks with positive values exceeding the number of tracks with negative values. While the component that arises from light quarks is almost symmetric, the  $c$  component has a moderate asymmetry and the  $b$  component shows a marked asymmetry. The asymmetry seen at  $|\delta| > 0.1 \text{ cm}$  is mainly due to decays of long lived strange particles such as  $K_S^0$ . In order to reduce the effects of the strange component, tracks with  $|\delta| > 0.1 \text{ cm}$  are rejected. The significance, defined as the ratio of the impact parameter  $\delta$  to its error, is shown in figure 2b for all selected tracks with  $|\delta| < 0.1 \text{ cm}$ .

The distributions of  $S_1$  (figure 2c) and of  $S_2$  (figure 2d) show the significance of the selected track in jets with exactly one selected track associated to the jet ( $S_1$ ) and the significance of the track with the second highest absolute significance in jets with two or more selected tracks ( $S_2$ ). For jets contributing to the distribution of  $S_2$  it is required that the tracks with the first and second highest absolute significance in the jet have the same sign of  $\delta$ . At moderate and large values of  $S_2$  the beauty contribution exceeds that from charm.

In order to substantially reduce the uncertainty due to the resolution of  $\delta$  and the light quark normalisation the negative bins in the  $S_1$  and  $S_2$  distributions are subtracted from the positive ones. These subtracted  $S_1$  and  $S_2$  distributions are shown in figures 2e and f. The distributions are dominated by charm quark events, with an increasing fraction of beauty quark events towards larger values of significance. The contribution from light quarks is seen to be small.

The  $c$ ,  $b$  and light quark fractions in the data are extracted using a simultaneous least squares fit of simulated reference distributions for  $c$ ,  $b$  and light quark events, obtained from the PYTHIA Monte Carlo simulation, to the measured subtracted  $S_1$  and  $S_2$  distributions (figures 2e and f). The total number of events before any CST track selection is also used in the fit. The Monte Carlo contributions from charm, beauty and light quark events are scaled by factors  $P_c$ ,  $P_b$  and  $P_l$  respectively, which are the free parameters of the fit. Only the statistical errors of the data and the Monte Carlo simulation are taken into account. The fit to the complete data sample gives scale factors  $P_c = 1.45 \pm 0.14$ ,  $P_b = 1.98 \pm 0.22$ , and  $P_l = 1.44 \pm 0.05$  and has a  $\chi^2/n.d.f.$  of 13.1/18. The Monte Carlo distributions shown in figures 1, 2, 6 and 7 are scaled by these factors. Consistent results are found when alternative methods are used to separate the quark flavours, such as the explicit reconstruction of secondary vertices described in section 7.

## 5 Calculations in Perturbative QCD

The Monte Carlo simulation programs PYTHIA [18] and CASCADE [20] provide cross section predictions in pQCD at leading order. Parton showers are implemented to account for higher order effects. PYTHIA uses the DGLAP parton evolution equations [21] while CASCADE contains an implementation of the CCFM evolution equations [22].

PYTHIA is run in an inclusive mode (MSTP(14)=30 [18]) in which direct and resolved photon processes, including heavy quark excitation, are generated using massless matrix elements for all quark flavours. The CTEQ5L [23] parton densities are used for the proton and those of SaS1D [24] for the photon. The charm and beauty quark masses are set to 1.5 and 4.75 GeV respectively, and the fragmentation is modelled by the Lund string model [25], using the Peterson function [26] for the longitudinal fragmentation of beauty and charm quarks.

Additional Monte Carlo samples of charm, beauty and light quark events are generated using the Monte Carlo generator CASCADE with the charm and beauty masses as used in PYTHIA. The process  $\gamma g \rightarrow c\bar{c}$  or  $b\bar{b}$  is implemented using off-shell matrix elements convoluted with  $k_t$  unintegrated parton distributions in the proton. In this analysis the parametrisation A0 [27] is used for the parton distributions.

QCD calculations to next-to-leading order are performed using the program FMNR [28]. FMNR implements the calculation at fixed order in the massive scheme, i.e. charm and beauty



quarks are generated dynamically in the hard process via boson–gluon fusion diagrams and the parton distributions for the proton and the photon consist only of light quarks ( $uds$ ) and gluons. FMNR provides weighted parton level events with two or three outgoing partons, i.e. the heavy quark antiquark pair and possibly a third parton. Values of 1.5 and 4.75 GeV are chosen for the  $c$  and  $b$  quark masses respectively. The renormalisation and factorisation scales are set to the transverse masses  $m_t = \sqrt{m_q^2 + p_{t,q\bar{q}}^2}$ , where  $p_{t,q\bar{q}}^2$  is the average of the squared transverse momenta of the heavy quark and anti-quark. The CTEQ5F3 parameterisation [23] is used for the parton distribution functions in the proton. Contributions from processes with resolved photons are calculated using the GRV-G HO distributions of partons in the photon [29]. In the next-to-leading order prediction these contributions are found to be small ( $\sim 3\%$ ).

In order to compare the parton level calculation with the data, corrections from parton to hadron level are applied which are determined using the PYTHIA Monte Carlo event generator. The jets at both the parton and the hadron level are reconstructed using the inclusive  $k_t$  jet-algorithm in the  $p_t$  recombination scheme. The bin-by-bin corrections from parton to hadron level are found to be less than  $\pm 10\%$  everywhere except in the bins  $0.7 < x_\gamma^{\text{obs}} < 0.85$  and  $0.85 < x_\gamma^{\text{obs}} < 1$  where the corrections are about  $+35\%$  and  $-15\%$  respectively.

Theoretical uncertainties of the NLO calculation are estimated by independent variations of the renormalisation and factorisation scales by factors of one half and two, and the maximal changes to the cross section predictions of  $30 - 35\%$  for charm and  $20 - 30\%$  for beauty are taken as systematic errors. The  $c$  ( $b$ ) masses are varied between 1.4 and 1.6 (4.5 and 5) GeV leading to cross section changes of up to  $\pm 4\%$ . The cross section variations when using other proton structure functions such as CTEQ6M [30], MRSG or MRST1 [31] are less than  $8\%$  in all regions of the measurement. The latter uncertainty is added in quadrature to the uncertainties from the scales and the quark mass.

## 6 Cross Section Measurement

For the measurement of the charm and beauty cross sections, the scale factors  $P_c$  and  $P_b$ , which are determined from fits of the subtracted significance distributions to the data, are multiplied with the cross section predictions of the PYTHIA Monte Carlo simulation. For the measurement of the differential charm and beauty cross sections the fit is performed separately in each bin  $i$ . The resulting scale factors  $P_{c,i}$  and  $P_{b,i}$  are then multiplied with the bin-averaged cross section predictions of the PYTHIA Monte Carlo simulation, divided by the respective bin size. In addition, the measured differential cross sections for charm and beauty dijet production are divided by the corresponding flavour inclusive cross sections to obtain the fractional contributions of events containing charm and beauty quarks. The flavour inclusive dijet cross section is measured by correcting the observed number of events before track selections for detector efficiencies and acceptances and dividing by the integrated luminosity.

### 6.1 Systematic Uncertainties

Systematic uncertainties of the cross section measurement are evaluated by variations applied to the Monte Carlo simulations. The resulting systematic uncertainties of the total charm and beauty dijet cross sections are listed in table 1 and detailed below.

Source	Variation	Uncertainty [%]	
		Charm	Beauty
Impact parameter resolution	$\oplus 25\mu\text{m}$ $\oplus 200\mu\text{m}$	7	10
Jet axis $\phi$ direction	$1^\circ$ shift in $\phi$	3	2
Track finding efficiency	$2\% \oplus 1\%$	3	8
$uds$ asymmetry	$\pm 50\%$	1	6
HQ production model (PYTHIA)	resolved $\gamma$ , $p_t$ dependence	7	14
Fragmentation model	Peterson / Lund	1	2
Fragmentation fractions	PDG	0.5	1.6
Hadron lifetimes	PDG	0.1	0.3
Charged track multiplicities	MARK-III, LEP, SLD	1.5	4
Jet energy scale	$2\%$	6	5
Trigger efficiency		5	5
Luminosity measurement		1.5	1.5
Total		14	22

Table 1: Systematic uncertainties of the measured total charm and beauty dijet cross sections.

- An uncertainty in the  $\delta$  resolution of the tracks is estimated by varying the resolution by an amount that encompasses the differences between the data and simulation (figure 2). This is achieved by applying an additional Gaussian smearing in the Monte Carlo simulation of  $200\mu\text{m}$  to  $5\%$  of randomly selected tracks and of  $25\mu\text{m}$  to the rest.
- The uncertainty of the jet axis reconstruction is estimated by shifting the jet axis in azimuth  $\phi$  by  $\pm 1^\circ$ .
- The reconstruction efficiency of central drift chamber tracks is uncertain to the level of  $2\%$  and the efficiency for these tracks to have hits in both  $r$ - $\phi$  layers of the silicon vertex detector is known to  $1\%$ .
- The uncertainty resulting from the shape of the subtracted significance distributions  $S_1$  and  $S_2$  for light quarks (figures 2e and f) is estimated by repeating the fits with the light quark  $S_1$  and  $S_2$  distributions varied by  $\pm 50\%$  of the default value.
- The systematic error arising from the uncertainty of the underlying physics model is estimated by varying the contribution from resolved photon processes in the PYTHIA prediction by  $\pm 50\%$ , and by reweighting the  $p_t$  distribution as predicted by PYTHIA to that of CASCADE. These variations lead to changes of the cross sections of  $\pm 7\%$  for charm and  $\pm 14\%$  for beauty.
- The uncertainties in the description of the heavy quark fragmentation are estimated by repeating the fits with Monte Carlo simulation templates in which the Lund Bowler function [25] is used for the longitudinal fragmentation instead of the Peterson function.
- The uncertainties arising from the various  $D$  and  $B$  hadron lifetimes, fragmentation fractions and mean charged track multiplicities are estimated by varying the input values of

the Monte Carlo simulation by the experimental errors of the corresponding measurements or world averages. For the fragmentation fractions of  $c$  and  $b$  quarks to hadrons and for the lifetimes of these hadrons the central values and errors on the world averages are taken from [32]. For the mean charged track multiplicities the values and uncertainties for  $c$  hadrons are taken from Mark-III [33] and for  $b$  hadrons from LEP and SLD measurements [34].

- The uncertainty of the jet energy scale of 2% leads to cross section uncertainties between 3% at small  $p_t^{\text{jet}}$  and 12% at large  $p_t^{\text{jet}}$  and 6% on average, independently of the quark flavour.
- The trigger efficiency is studied using monitoring events from neutral current processes in deep inelastic scattering in which the scattered positron triggers the events independently of the triggers under study. The uncertainty is determined to be 5%.
- The luminosity is known to an accuracy of 1.5%.

Total systematic uncertainties of 14% and 22% are obtained for the measurement of the charm and the beauty production cross sections respectively. The total systematic error for the flavour inclusive dijet cross section is 8% resulting from the uncertainty of the hadronic energy scale (6%), the trigger efficiency uncertainty (5%) and the uncertainty of the luminosity measurement (1.5%). For the relative contributions of charm and beauty production to the flavour inclusive dijet cross section, the statistical errors are added in quadrature and the systematic errors include those sources that are specific to the charm and beauty cross section measurement. The same uncertainties are equally attributed to all bins of the measurement except for the uncertainty of the hadronic energy scale for which the uncertainties are determined and applied individually in each bin of the measurement.

## 6.2 Results

The total dijet charm photoproduction cross section in the range  $Q^2 < 1 \text{ GeV}^2$ ,  $0.15 < y < 0.8$ ,  $p_t^{\text{jet}_{1(2)}} > 11(8) \text{ GeV}$  and  $-0.9 < \eta^{\text{jet}_{1(2)}} < 1.3$  is measured to be

$$\sigma(ep \rightarrow ec\bar{c}X \rightarrow ejjX) = 702 \pm 67(\text{stat.}) \pm 95(\text{syst.})\text{pb.}$$

For the same kinematic range, the measured beauty cross section is

$$\sigma(ep \rightarrow eb\bar{b}X \rightarrow ejjX) = 150 \pm 17(\text{stat.}) \pm 33(\text{syst.})\text{pb.}$$

The predictions from the theoretical calculations are detailed in table 2. The NLO parton level calculations are corrected to the hadron level using correction factors as determined from PYTHIA (see section 5). For charm, the NLO QCD calculation FMNR is somewhat lower than the measurement but still in reasonable agreement within the theoretical errors. For beauty, FMNR is lower than the data by a factor 1.8, corresponding to 1.6 standard deviations, taking both experimental uncertainties and uncertainties in the theory into account. For both, charm and beauty, PYTHIA and CASCADE predict a normalisation which is similar to that of FMNR.

	Charm [pb]	Beauty [pb]
Data	$702 \pm 67(stat.) \pm 95(syst.)$	$150 \pm 17(stat.) \pm 33(syst.)$
FMNR	$500^{+173}_{-99}$	$83^{+19}_{-14}$
PYTHIA	484	76
CASCADE	438	80

Table 2: The measured charm and beauty photoproduction dijet cross sections in the kinematic range  $Q^2 < 1 \text{ GeV}^2$ ,  $0.15 < y < 0.8$ ,  $p_t^{\text{jet}_{1(2)}} > 11(8) \text{ GeV}$  and  $-0.9 < \eta^{\text{jet}_{1(2)}} < 1.3$  in comparison to predictions in NLO QCD (FMNR) and from the Monte Carlo programs PYTHIA and CASCADE.

The measured differential cross sections as functions of  $p_t^{\text{jet}_1}$ , of  $\bar{\eta}$  and of  $x_\gamma^{\text{obs}}$ , are shown in figure 3 and listed in table 3. PYTHIA is used to determine the point in the bin at which the bin-averaged cross section equals the differential cross section. Both the charm and beauty data are reasonably well described in shape. A large difference, however, between the beauty data and the NLO QCD calculation is observed in the region of small values of  $x_\gamma^{\text{obs}}$  (figure 3f), where the prediction lies significantly below the data. In this region, PYTHIA predicts a large contribution from events with resolved photons, as indicated in the figures by the dashed-dotted lines. PYTHIA describes the shapes of the charm and beauty data distributions, while the normalisations are low. The CASCADE prediction is too small in the region of small  $x_\gamma^{\text{obs}}$ , but approaches the measurement in the region  $x_\gamma^{\text{obs}} > 0.85$ .

Differential cross sections are also measured separately for the region  $x_\gamma^{\text{obs}} > 0.85$  and the results as functions of  $p_t^{\text{jet}_1}$  and of  $\bar{\eta}$  are shown in figure 4 and listed in table 4. The charm cross sections are in good agreement with the NLO QCD calculation both in normalisation and shape. The beauty cross sections are also reasonably well described, the agreement being significantly better than for the whole range of  $x_\gamma^{\text{obs}}$ .

The relative contributions from charm and beauty to the inclusive dijet cross sections are presented in figure 5 and listed in tables 3 and 4. In figure 5a, the relative contributions are shown as a function of  $x_\gamma^{\text{obs}}$ . The data are compared with the PYTHIA Monte Carlo simulation which predicts an increase of the relative charm and beauty contributions towards large  $x_\gamma^{\text{obs}}$  where direct photon-gluon fusion processes dominate.

Assuming the charm and beauty quarks to be light, naïve quark charge counting predicts a value of four for the relative production rates of charm to beauty dijets in direct photon-gluon fusion processes. In comparison, the measurement in the region  $x_\gamma^{\text{obs}} > 0.85$  yields a ratio of  $5.1 \pm 1.1$  (stat.). In figure 5b and c the relative contributions to the dijet cross section are shown for the region  $x_\gamma^{\text{obs}} > 0.85$  as a function of  $p_t^{\text{jet}_1}$  and of  $\bar{\eta}$ . The ratios are constant within their uncertainties.

## 7 Heavy Quark Enriched Data Sample

In order to study the description of the data by the PYTHIA Monte Carlo further, a subsample of events is used, in which the fraction of events containing heavy quarks is enriched. For

this subsample secondary vertices of the heavy hadron decays are reconstructed explicitly using events with at least two selected tracks in a given jet. The relative fraction of heavy quarks in the event sample is then further enhanced by subsequent cuts on the secondary vertex track multiplicity and the decay length significance. For this heavy quark enriched sample the distributions of the jet transverse momentum, the mean pseudo-rapidity and the observable  $x_\gamma^{\text{obs}}$  are presented and the decomposition and shape differences of direct and resolved photon processes, as implemented in PYTHIA, are studied.

Using a method presented in a previous H1 publication [5] the primary vertex and the secondary vertices of the heavy hadron decays are reconstructed. For each jet the associated tracks are used to reconstruct a secondary vertex in an iterative procedure. No definite assignment of tracks to vertices is made, but each track is assigned a weight in the range 0 to 1 for each vertex candidate, using the weight function of [35]. The smaller the distance of the track to the vertex candidate, the larger the weight. For each jet the vertex configuration that minimises the global fit  $\chi^2$  is found iteratively using deterministic annealing [36]. The number of tracks which contribute with a weight greater than 0.8 to the secondary vertex is used as a measure of the decay vertex track multiplicity. The decay length significance is given by the transverse distance between the primary and the secondary vertex divided by its error. The sign is defined using the projection of the corresponding vector on the jet direction. Figure 6 shows the decay length significance distributions for different decay track multiplicities. Good agreement is seen between the data and the distributions from the PYTHIA Monte Carlo simulation which are scaled by the factors as obtained from the fit to the subtracted significance distributions  $S_1$  and  $S_2$ . Conversely, a simultaneous fit of the decay length significance distributions for the different track multiplicities gives results consistent with those from the subtracted significance distributions.

Figure 6 shows that in heavy quark events secondary vertices are significantly displaced in the direction of the related jet axis. Contributions from light quarks are mainly observed in the two-track sample at small decay length significances. In the two-track sample the contribution from charm and beauty is similar to that of light quark events while the three and four-track samples are dominated by the beauty component, as expected from the mean charged particle multiplicity in heavy hadron decays.

The fraction of events with heavy quarks is enhanced by requiring a secondary decay vertex with two or more tracks and a decay length significance larger than 2.0. Applying these cuts, the distributions for  $p_t^{\text{jet}_1}$ , for  $\bar{\eta}$  and for  $x_\gamma^{\text{obs}}$  are shown in figure 7. The data are compared to the PYTHIA Monte Carlo simulations. In figures 7a, c and e the decomposition into light, charm and beauty quark contributions is indicated. These are determined using the scale factors as obtained from the fit to the subtracted significance distributions of the full sample. Good agreement between the PYTHIA prediction and the data is seen. The contributions from charm and beauty events are 44% and 41% respectively, while 15% of the events contain only light quarks. In figures 7b, d and f the same data are shown together with the contributions from direct ( $\gamma g \rightarrow q\bar{q}$ ) and resolved processes, as predicted by the PYTHIA simulation. According to the leading order QCD calculation, as implemented in PYTHIA, the fraction of events that arise from processes with resolved photons is about 40%.

In the region  $x_\gamma^{\text{obs}} < 0.85$  the contribution from resolved processes is enhanced and amounts to about 80%. According to PYTHIA the contribution from processes with heavy quark excitation is by far dominant. In conclusion, the data are well described by the leading order Monte

Carlo simulation PYTHIA in which significant contributions from heavy quark excitation processes are predicted.

## 8 Conclusions

Differential charm and beauty dijet photoproduction cross sections at HERA are measured using a technique based on the lifetime of the heavy quark hadrons. The heavy quark cross sections are determined using the subtracted impact parameter significance distributions of tracks in dijet events. The cross sections are measured as functions of the transverse momentum  $p_t^{\text{jel}_1}$  of the leading jet, of the mean pseudo-rapidity  $\bar{\eta}$  of the two jets and of the observable  $x_\gamma^{\text{obs}}$ . Taking into account the theoretical uncertainties, the charm cross sections are consistent both in normalisation and shape with a calculation in perturbative QCD to next-to-leading order. The beauty cross sections tend to be higher than NLO, by  $1.6\sigma$  for the total cross section, with a more significant discrepancy observed in the region of  $x_\gamma^{\text{obs}} < 0.85$  where processes involving resolved photons or higher order contributions are expected to be enhanced. The Monte Carlo generator PYTHIA gives a good description of the shape of both the charm and the beauty data. The data confirm the expectation within this model that a significant contribution to the heavy quark dijet cross section comes from processes with resolved photons. In the region  $x_\gamma^{\text{obs}} > 0.85$ , the relative contributions from charm and beauty to the inclusive dijet cross section are found to be in agreement within errors with values of 4/11 and 1/11, i.e. the naïve expectation for the direct photon-gluon fusion process, assuming all quarks to be massless.

## Acknowledgements

We are grateful to the HERA machine group whose outstanding efforts have made this experiment possible. We thank the engineers and technicians for their work in constructing and maintaining the H1 detector, our funding agencies for financial support, the DESY technical staff for continual assistance and the DESY directorate for support and for the hospitality which they extend to the non-DESY members of the collaboration.

## References

- [1] S. Aid *et al.* [H1 Collaboration], Nucl. Phys. B **472** (1996) 32 [hep-ex/9604005].
- [2] J. Breitweg *et al.* [ZEUS Collaboration], Eur. Phys. J. C **6** (1999) 67 [hep-ex/9807008].
- [3] S. Chekanov *et al.* [ZEUS Collaboration], Phys. Lett. B **565** (2003) 87 [hep-ex/0302025].
- [4] S. Chekanov *et al.* [ZEUS Collaboration], Nucl. Phys. B **729** (2005) 492 [hep-ex/0507089].
- [5] A. Aktas *et al.* [H1 Collaboration], Eur. Phys. J. C **40** (2005) 349 [hep-ex/0411046].
- [6] A. Aktas *et al.* [H1 Collaboration], Eur. Phys. J. C **45** (2006) 23 [hep-ex/0507081].
- [7] C. Adloff *et al.* [H1 Collaboration], Phys. Lett. B **467** (1999) 156 [Erratum-ibid. B **518** (2001) 331] [hep-ex/9909029].
- [8] J. Breitweg *et al.* [ZEUS Collaboration], Eur. Phys. J. C **18** (2001) 625 [hep-ex/0011081].
- [9] S. Chekanov *et al.* [ZEUS Collaboration], Phys. Rev. D **70** (2004) 012008 [hep-ex/0312057].
- [10] A. Aktas *et al.* [H1 Collaboration], Eur. Phys. J. C **41** (2005) 453 [hep-ex/0502010].
- [11] I. Abt *et al.* [H1 Collaboration], Nucl. Instrum. Meth. A **386** (1997) 310 and 348.
- [12] D. Pitzl *et al.*, Nucl. Instrum. Meth. A **454** (2000) 334 [hep-ex/0002044].
- [13] T. Nicholls *et al.* [H1 SPACAL Group Collaboration], Nucl. Instrum. Meth. A **374** (1996) 149.
- [14] M. Peez, PhD Thesis, Univ. Lyon, 2003, available at <http://www-h1.desy.de/publications/theses.list.html>.
- [15] F. Jacquet, A. Blondel, in: Proc. *Study of an ep Facility for Europe* (ed. U. Amaldi), DESY 79/48, p 391 (1979).
- [16] S. Catani, Yu. Dokshitzer, M.H. Seymour and B.R. Webber, Nucl. Phys. B **406** (1993) 187.
- [17] Z. Kunszt, P. Nason, G. Marchesini and B.R. Webber, in: LEP Physics Workshop vol.1 (1989) 373.
- [18] T. Sjöstrand, Comput. Phys. Commun. **82** (1994) 74.
- [19] R. Brun *et al.*, CERN-DD/EE-84-1 (1987).
- [20] H. Jung and G. P. Salam, Eur. Phys. J. C **19** (2001) 351 [hep-ph/0012143];  
H. Jung, Comput. Phys. Commun. **143** (2002) 100 [hep-ph/0109102].

- [21] V.N. Gribov and L.N. Lipatov, *Yad. Fiz.* **15** (1972) 781 [*Sov. J. Nucl. Phys.* **15** (1972) 438]; G. Altarelli and G. Parisi, *Nucl. Phys. B* **126** (1977) 298; Y.L. Dokshitzer, *Sov. Phys. JETP* **46** (1977) 641 [*Zh. Eksp. Teor. Fiz.* **73** (1977) 1216].
- [22] M. Ciafaloni, *Nucl. Phys. B* **296** (1988) 49; S. Catani, F. Fiorani and G. Marchesini, *Phys. Lett. B* **234** (1990) 339; *idem*, *Nucl. Phys. B* **336** (1990) 18; G. Marchesini, *Nucl. Phys. B* **445** (1995) 49.
- [23] H. L. Lai *et al.*, *Eur. Phys. J. C* **12** (2000) 375 [hep-ph/9903282].
- [24] G.A. Schuler and T. Sjöstrand, *Phys. Lett. B* **376** (1996) 193 [hep-ph/9601282].
- [25] B. Andersson, G. Gustafson, G. Ingelman and T. Sjöstrand, *Phys. Rept.* **97** (1983) 31.
- [26] C. Peterson, D. Schlatter, I. Schmitt and P.M. Zerwas, *Phys. Rev. D* **27** (1983) 105.
- [27] H. Jung, hep-ph/0411287.
- [28] S. Frixione, M. L. Mangano, P. Nason and G. Ridolfi, *Phys. Lett. B* **348** (1995) 633 [hep-ph/9412348].
- [29] M. Glück, E. Reya and A. Vogt, *Phys. Rev. D* **45** (1992) 3986; *idem*, *Phys. Rev. D* **46** (1992) 1973 .
- [30] S. Kretzer, H. L. Lai, F. I. Olness and W. K. Tung, *Phys. Rev. D* **69** (2004) 114005 [hep-ph/0307022].
- [31] A.D. Martin, R.G. Roberts and W.J. Stirling, *Phys. Lett. B* **354** 155 (1995); A.D. Martin, R.G. Roberts, W.J. Stirling and R.S. Thorne, *Eur. Phys. J. C* **4** (1998) 463.
- [32] S. Eidelman *et al.* [Particle Data Group Collaboration], *Phys. Lett. B* **592** (2004) 1.
- [33] D. Coffman *et al.* [MARK-III Collaboration], *Phys. Lett. B* **263** (1991) 135.
- [34] D. Abbaneo *et al.* [LEP/SLD Heavy Flavour Working Group], LEPHF 2001-01, available from <http://lepewwg.web.cern.ch/LEPEWWG/heavy/>
- [35] R. Frühwirth *et al.*, *Nucl. Instrum. Meth. A* **502** (2003) 446.
- [36] R. Frühwirth and A. Strandlie, *Comput. Phys. Commun.* **120** (1999) 197.



			Charm					
$p_t^{\text{jet}_1}$ range [GeV]	$\langle p_t^{\text{jet}_1} \rangle$ [GeV]		$d\sigma/dp_t^{\text{jet}_1}$ [pb/GeV]	stat.	syst.	$f^{c\bar{c}}$	stat.	syst.
11.0 14.5	12.75		137	20	20	0.333	0.048	0.044
14.5 18.0	16.25		49.5	7.6	7.9	0.352	0.054	0.046
18.0 22.5	20.0		10.6	2.5	1.8	0.270	0.062	0.035
22.5 35.0	27.0		2.46	0.86	0.45	0.402	0.140	0.052
$\bar{\eta}$ range	$\langle \bar{\eta} \rangle$		$d\sigma/d\bar{\eta}$ [pb]	stat.	syst.	$f^{c\bar{c}}$	stat.	syst.
-0.90 0.10	-0.35		162	24	22	0.337	0.051	0.045
0.10 0.60	0.35		674	86	101	0.346	0.044	0.045
0.60 1.30	0.95		386	52	61	0.358	0.049	0.047
$x_\gamma^{\text{obs}}$ range	$\langle x_\gamma^{\text{obs}} \rangle$		$d\sigma/dx_\gamma^{\text{obs}}$ [pb]	stat.	syst.	$f^{c\bar{c}}$	stat.	syst.
0.10 0.70	0.45		236	70	34	0.250	0.074	0.033
0.70 0.85	0.77		1017	271	162	0.342	0.091	0.047
0.85 1.00	0.92		2994	280	498	0.374	0.035	0.049

			Beauty					
$p_t^{\text{jet}_1}$ range [GeV]	$\langle p_t^{\text{jet}_1} \rangle$ [GeV]		$d\sigma/dp_t^{\text{jet}_1}$ [pb/GeV]	stat.	syst.	$f^{b\bar{b}}$	stat.	syst.
11.0 14.5	12.75		24.7	6.1	5.5	0.060	0.015	0.013
14.5 18.0	16.25		9.79	1.87	2.15	0.070	0.013	0.015
18.0 22.5	20.0		3.37	0.48	0.78	0.085	0.012	0.018
22.5 35.0	27.0		0.28	0.14	0.07	0.046	0.022	0.010
$\bar{\eta}$ range	$\langle \bar{\eta} \rangle$		$d\sigma/d\bar{\eta}$ [pb]	stat.	syst.	$f^{b\bar{b}}$	stat.	syst.
-0.90 0.10	-0.35		37.1	5.9	7.8	0.077	0.012	0.016
0.10 0.60	0.35		112	17	25	0.057	0.009	0.012
0.60 1.30	0.95		56.2	11.3	12.4	0.052	0.010	0.011
$x_\gamma^{\text{obs}}$ range	$\langle x_\gamma^{\text{obs}} \rangle$		$d\sigma/dx_\gamma^{\text{obs}}$ [pb]	stat.	syst.	$f^{b\bar{b}}$	stat.	syst.
0.10 0.70	0.45		44.6	12.8	9.9	0.047	0.014	0.010
0.70 0.85	0.77		191	60	44	0.064	0.020	0.014
0.85 1.00	0.92		584	72	135	0.073	0.009	0.015

Table 3: The measured charm and beauty dijet photoproduction cross sections and the relative contributions  $f^{c\bar{c}}$  and  $f^{b\bar{b}}$  to the inclusive dijet photoproduction cross section with statistical and systematic errors.

		Charm						
$p_t^{\text{jet}_1}$ range [GeV]	$\langle p_t^{\text{jet}_1} \rangle$ [GeV]	$d\sigma/dp_t^{\text{jet}_1}$ [pb/GeV]	stat.	syst.	$f^{c\bar{c}}$	stat.	syst.	
11.0 14.5	12.75	73.3	12.7	10.7	0.348	0.060	0.046	
14.5 18.0	16.25	29.0	4.6	4.6	0.364	0.057	0.048	
18.0 22.5	20.0	8.79	1.75	1.46	0.357	0.071	0.047	
22.5 35.0	27.0	1.94	0.70	0.35	0.455	0.165	0.060	
$\bar{\eta}$ range	$\langle \bar{\eta} \rangle$	$d\sigma/d\bar{\eta}$ [pb]	stat.	syst.	$f^{c\bar{c}}$	stat.	syst.	
-0.90 0.10	-0.35	115	21	16	0.322	0.058	0.043	
0.10 0.60	0.35	496	70	74	0.462	0.065	0.060	
0.60 1.30	0.95	165	24	26	0.374	0.055	0.049	

		Beauty						
$p_t^{\text{jet}_1}$ range [GeV]	$\langle p_t^{\text{jet}_1} \rangle$ [GeV]	$d\sigma/dp_t^{\text{jet}_1}$ [pb/GeV]	stat.	syst.	$f^{b\bar{b}}$	stat.	syst.	
11.0 14.5	12.75	15.3	4.3	3.4	0.073	0.020	0.015	
14.5 18.0	16.25	6.19	1.20	1.42	0.078	0.015	0.016	
18.0 22.5	20.0	1.89	0.31	0.44	0.076	0.013	0.016	
22.5 35.0	27.0	0.27	0.18	0.07	0.063	0.043	0.014	
$\bar{\eta}$ range	$\langle \bar{\eta} \rangle$	$d\sigma/d\bar{\eta}$ [pb]	stat.	syst.	$f^{b\bar{b}}$	stat.	syst.	
-0.90 0.10	-0.35	29.8	4.7	6.3	0.084	0.013	0.018	
0.10 0.60	0.35	54.4	15.5	12.0	0.051	0.014	0.011	
0.60 1.30	0.95	31.9	5.7	7.1	0.072	0.013	0.016	

Table 4: The measured charm and beauty dijet photoproduction cross sections and the relative contributions  $f^{c\bar{c}}$  and  $f^{b\bar{b}}$  to the inclusive photoproduction dijet cross section for the region  $x_\gamma^{\text{obs}} > 0.85$  with statistical and systematic errors.

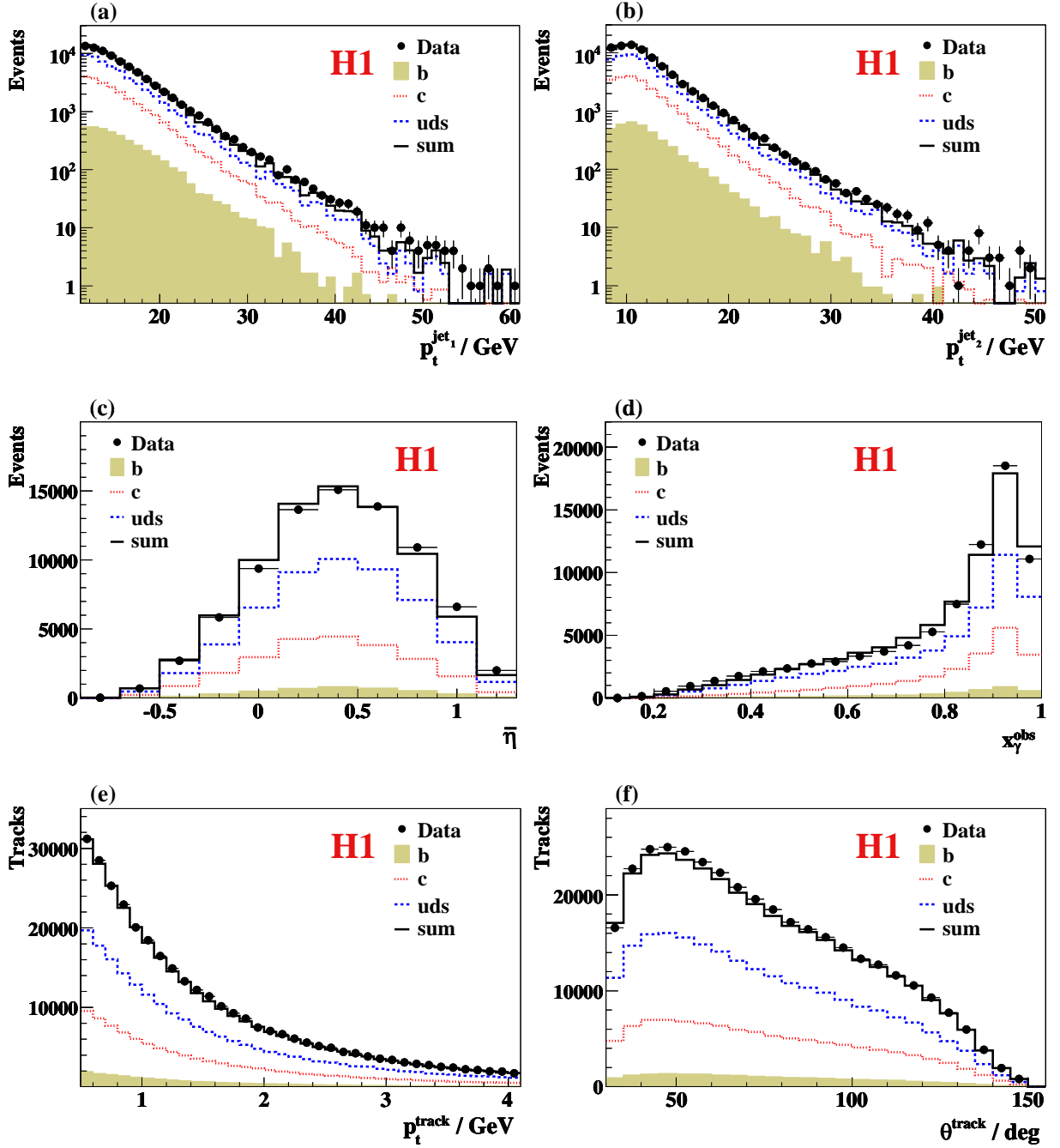


Figure 1: Distributions of a) the transverse momentum  $p_t^{\text{jet}_1}$  of the leading jet, b) the transverse momentum  $p_t^{\text{jet}_2}$  of the second jet, c) the mean pseudo-rapidity  $\bar{\eta}$  of the two jets, d) the observable  $x_\gamma^{\text{obs}}$ , e) the transverse momentum of the selected tracks and f) the polar angle of the selected tracks. The expectation from the PYTHIA Monte Carlo simulation is included in the figure, showing the contributions from the various quark flavours after applying the scale factors obtained from the fit to the subtracted significance distributions of the data (see section 4).

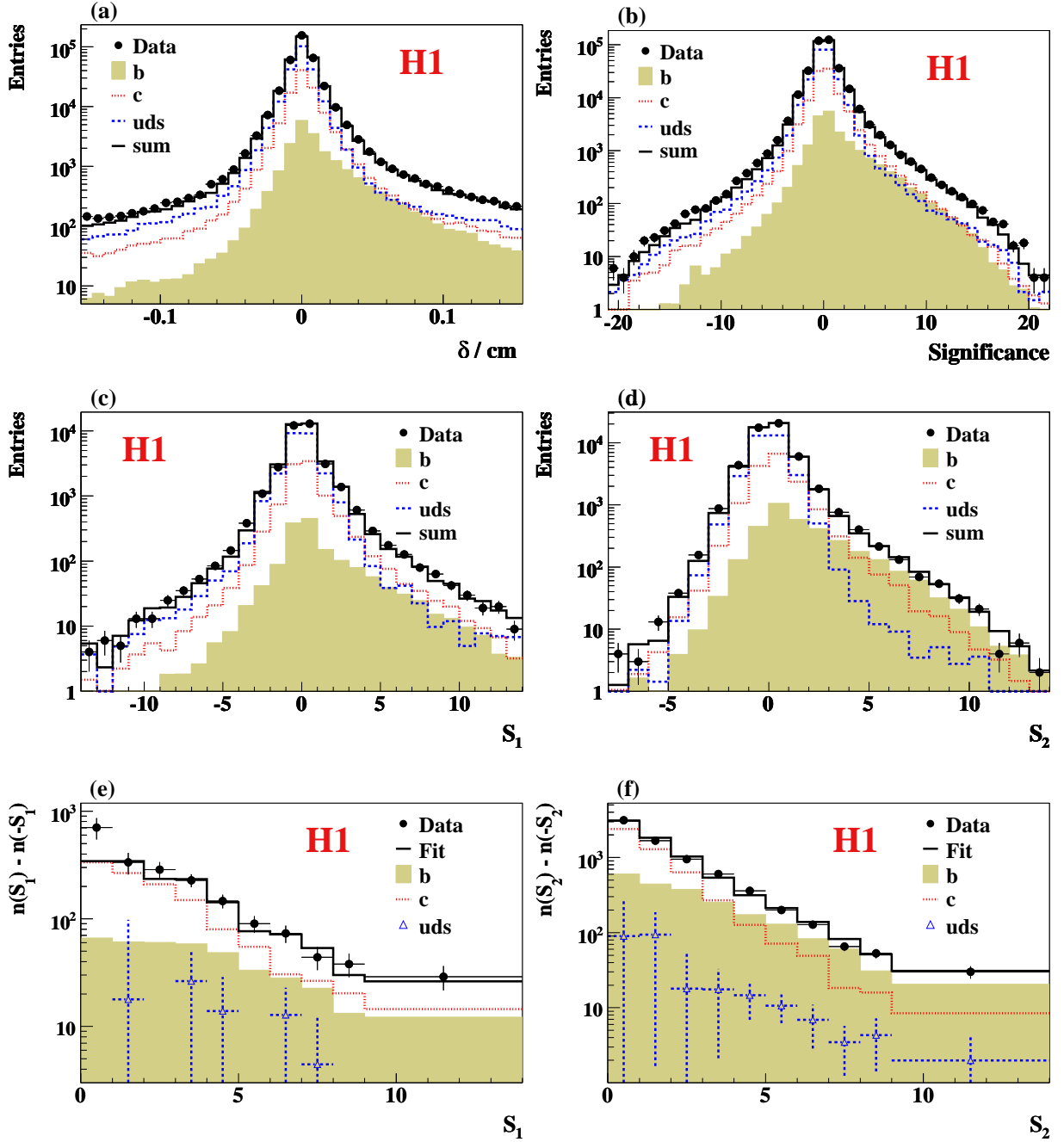


Figure 2: Distributions of a) the signed impact parameter  $\delta$  of selected tracks, b) the signed significance, c) the significance  $S_1$  of tracks in jets with exactly one selected track, d) the significance  $S_2$  of the track with the second highest significance in jets with two or more selected tracks, e) the subtracted signed significance for the sample with exactly one selected track, f) the subtracted signed significance for the sample with two or more selected tracks. In b) to f) only tracks with an impact parameter  $|\delta| < 0.1$  cm are considered. The expectation from the PYTHIA Monte Carlo simulation is included in the figure, showing the contributions from the various quark flavours after applying the scale factors obtained from the fit to the subtracted significance distributions of the data (see section 4).

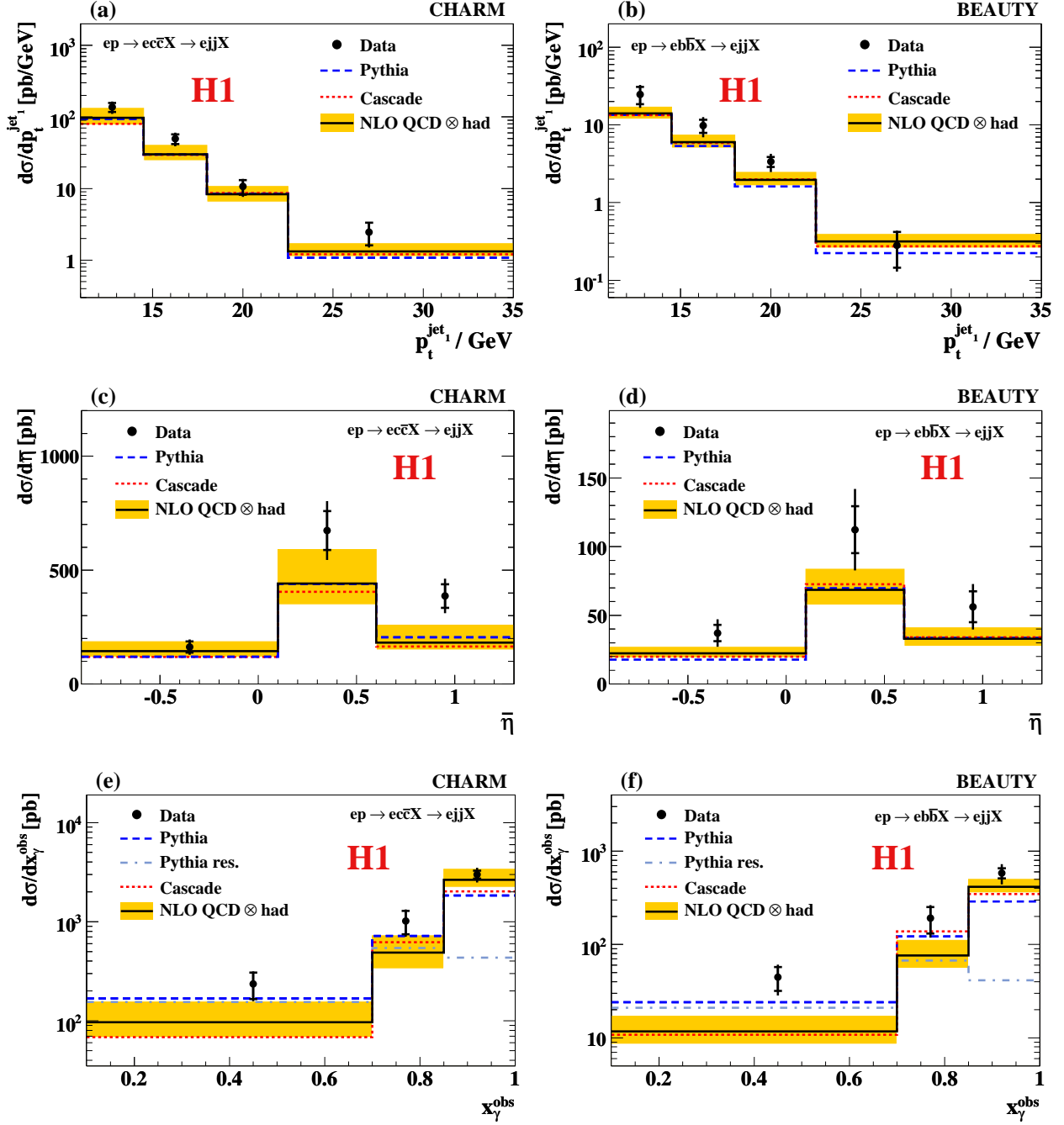


Figure 3: Differential charm and beauty photoproduction cross sections a,b)  $d\sigma/dp_t^{\text{jet}_1}$ , c,d)  $d\sigma/d\eta$  and e,f)  $d\sigma/dx_\gamma^{\text{obs}}$  for the process  $ep \rightarrow e(c\bar{c} \text{ or } b\bar{b})X \rightarrow ejjX$ . The inner error bars indicate the statistical uncertainty and the outer error bars show the statistical and systematic errors added in quadrature. The solid lines indicate the prediction from a NLO QCD calculation, corrected for hadronisation effects, and the shaded band shows the estimated uncertainty. The absolute predictions from PYTHIA (dashed lines) and CASCADE (dotted lines) are also shown. The contribution from resolved processes in PYTHIA (dash-dotted lines) is depicted separately. The contribution from resolved processes in PYTHIA (dash-dotted lines) is depicted separately.

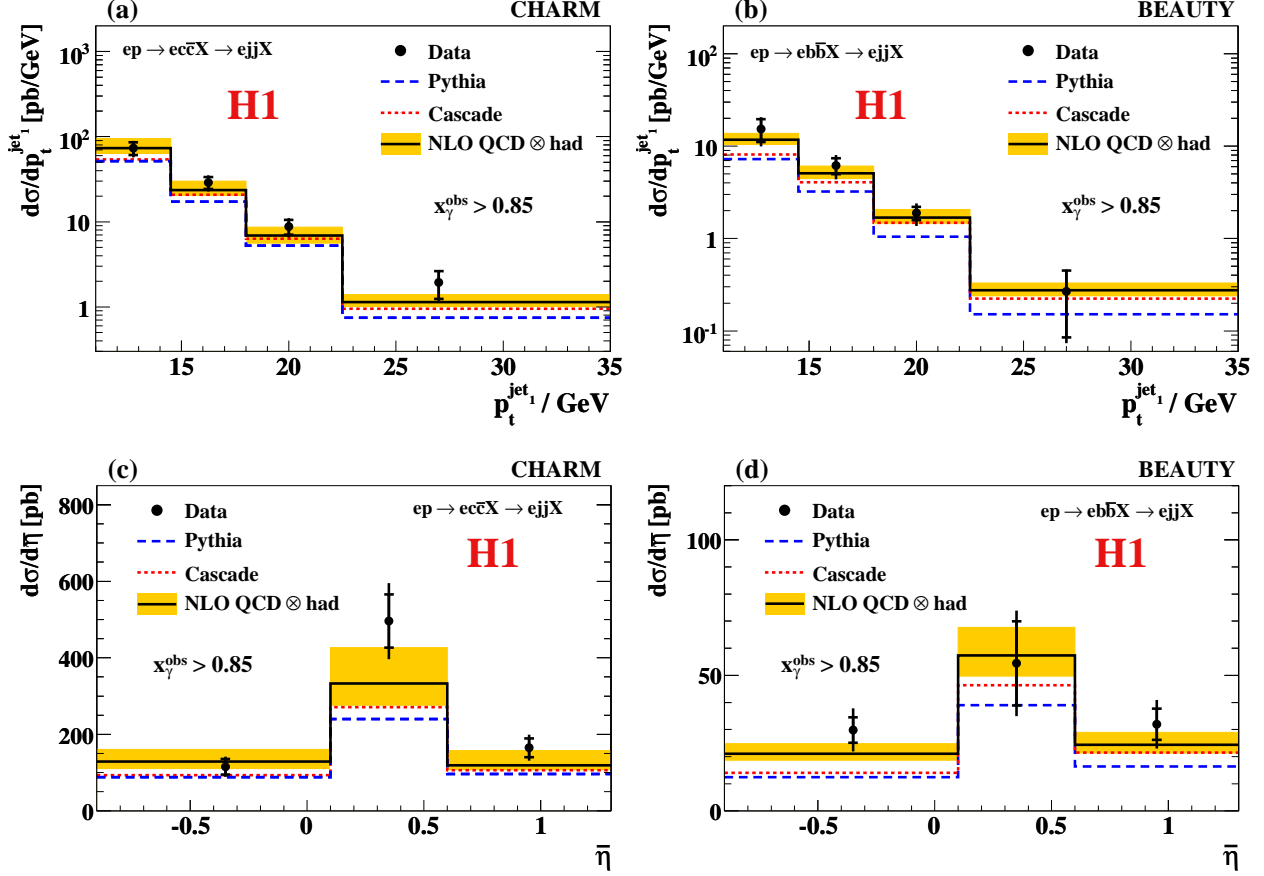


Figure 4: Differential charm and beauty photoproduction cross sections a,b)  $d\sigma/dp_t^{\text{jet}_1}$  and c,d)  $d\sigma/d\eta$  for the process  $ep \rightarrow e(c\bar{c} \text{ or } b\bar{b})X \rightarrow ejjX$  in the region  $x_\gamma^{\text{obs}} > 0.85$ . The inner error bars indicate the statistical uncertainty and the outer error bars show the statistical and systematic errors added in quadrature. The solid lines indicate the prediction from a NLO QCD calculation, corrected for hadronisation effects, and the shaded band shows the estimated uncertainty. The absolute predictions from PYTHIA (dashed lines) and CASCADE (dotted lines) are also shown.

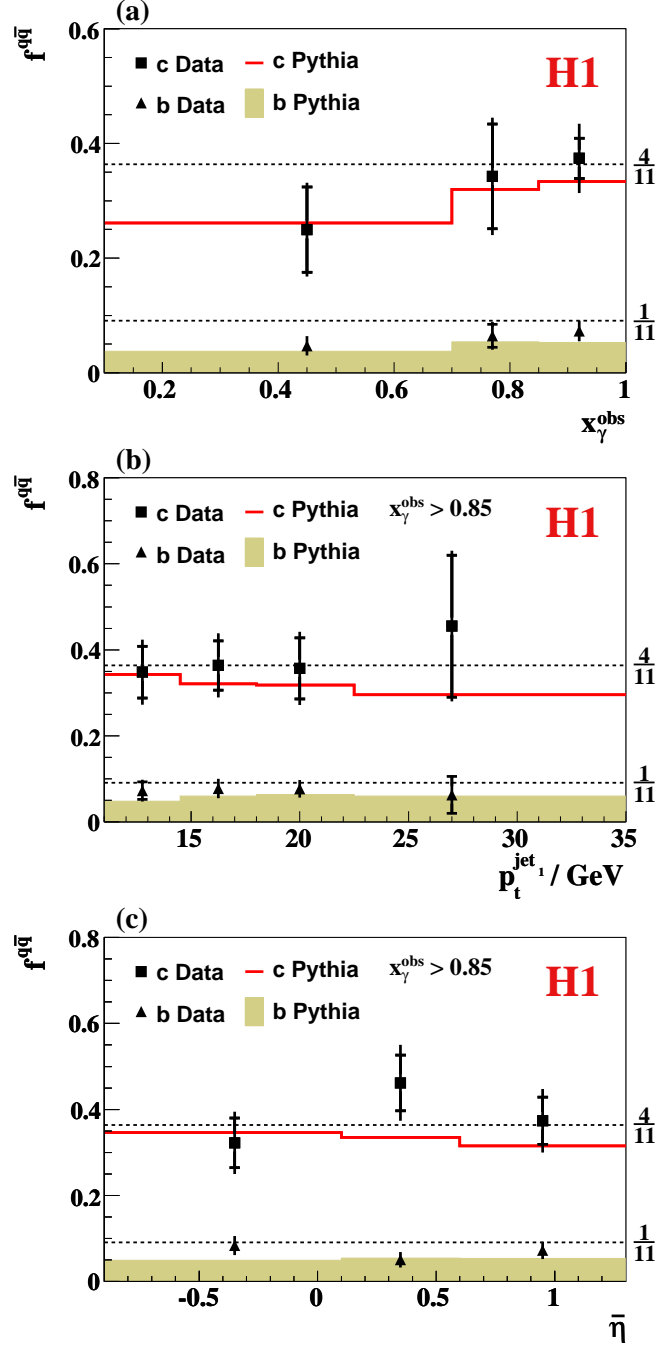


Figure 5: Relative contributions from charm (squares) and beauty events (triangles) as a function of a) the observable  $x_\gamma^{obs}$ , b) the transverse momentum  $p_t^{jet1}$  of the leading jet for  $x_\gamma^{obs} > 0.85$  and c) the mean pseudo-rapidity  $\bar{\eta}$  of the two jets for  $x_\gamma^{obs} > 0.85$ . The inner error bars indicate the statistical uncertainty and the outer error bars show the statistical and systematic error added in quadrature. The solid line (shaded area) indicates the absolute prediction from PYTHIA for charm (beauty).

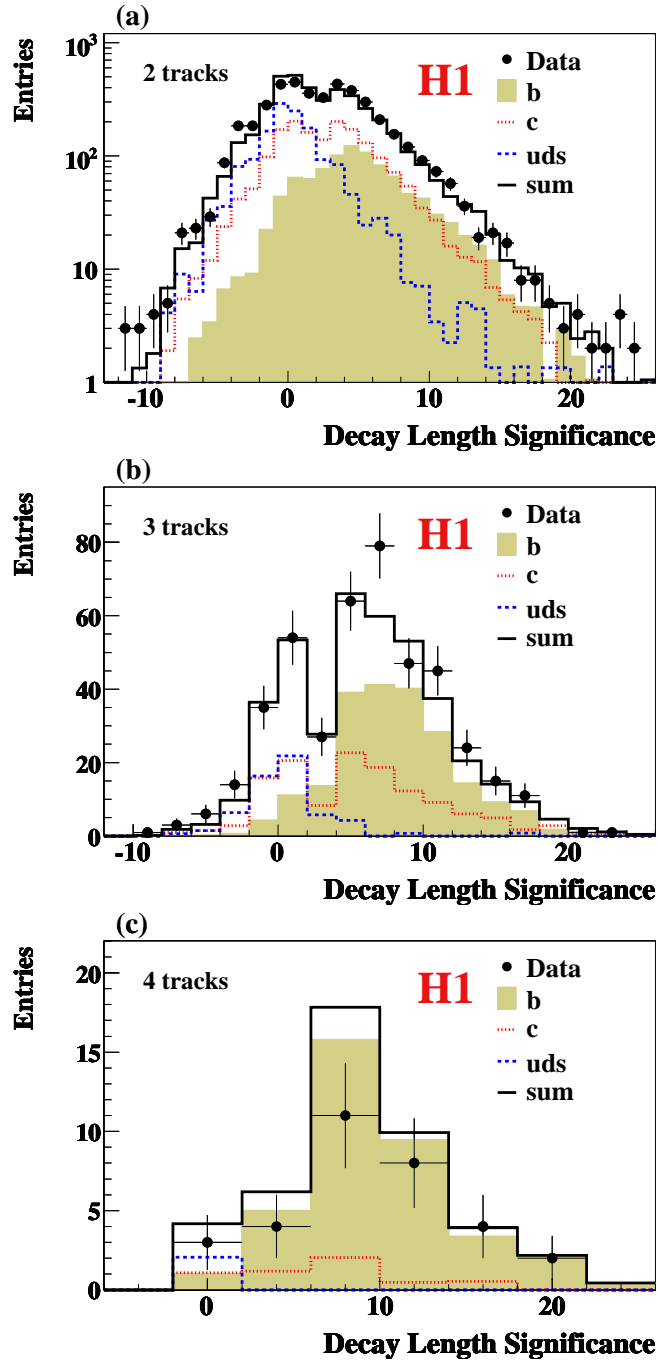


Figure 6: Decay length significance distributions for samples of events with a secondary vertex reconstructed from a) 2, b) 3 and c) 4 tracks. The data (points) are compared with the PYTHIA simulation after applying the scale factors as obtained from the fit to the subtracted significance distributions of the full sample.



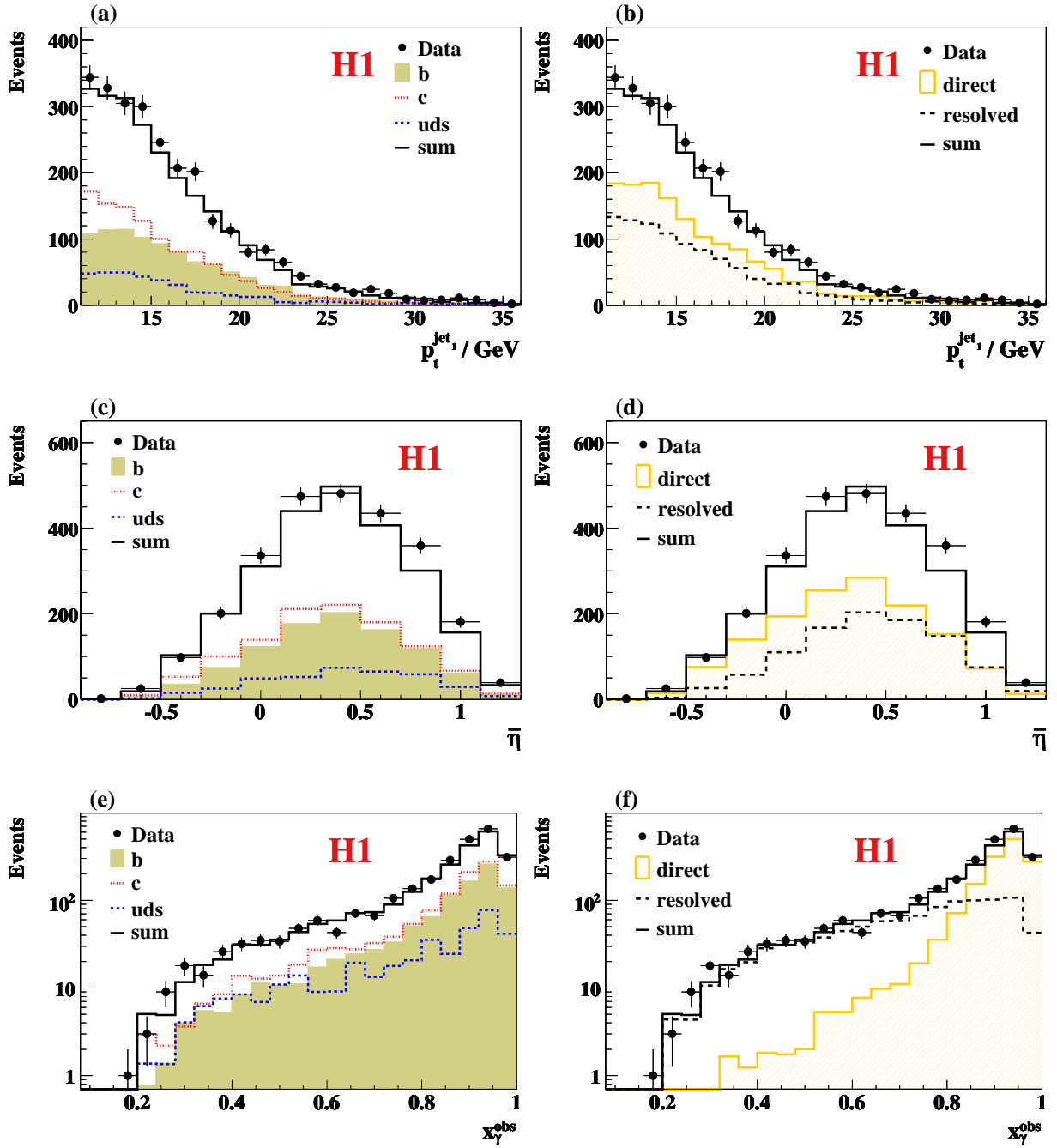


Figure 7: Distributions of the heavy quark enriched sample with two or more tracks originating from a secondary vertex and a decay length significance larger than 2.0 (see text). The data are compared to the PYTHIA simulation for the distributions of a,b) the transverse momentum  $p_t^{\text{jet}_1}$  of the leading jet, c,d) the mean pseudo-rapidity  $\bar{\eta}$  of the two jets and e,f) the observable  $x_\gamma^{\text{obs}}$ . The left column shows the decomposition of the distribution into beauty, charm and light quarks after scaling the PYTHIA predictions by the scale factors obtained from the fit to the subtracted significance distributions of the full sample. In the right column the contributions from direct and resolved processes in PYTHIA are indicated as shaded histogram and dashed line respectively.